Optical and Chemical Characterization of Aerosols Emitted from Coal, Heavy and Light Fuel Oil, and Small-Scale Wood Combustion

Anna K. Frey,[*,†] Karri Saarnio,[†] Heikki Lamberg,[‡] Fanni Mylläri,[§] Panu Karjalainen,[§] Kimmo Teinilä,[†] Samara Carbone,[†] Jarkko Tissari,[‡] Ville Niemelä,[∥] Anna Häyrinen,[⊥] Jani Rautiainen,[⊥] Jorma Kytömäki,[⊥] Paulo Artaxo,[#] Aki Virkkula,[†] Liisa Pirjola,[▽] Topi Rönkkö,[§] Jorma Keskinen,[§] Jorma Jokiniemi,[‡,○] and Risto Hillamo[†]

[†]Air Quality, Finnish Meteorological Institute, P.O. Box 503, FI-00101 Helsinki, Finland

[‡]Fine Particle and Aerosol Technology Laboratory, Department of Environmental Science, University of Eastern Finland, P.O. Box 1627, FI-70211 Kuopio, Finland

[§]Department of Physics, Tampere University of Technology, P.O. Box 692, FI-33101 Tampere, Finland

[∥]Dekati Ltd., Tykkitie 1, FI-36240 Kangasala, Finland

[⊥]Helsingin Energia Plc, FI-00090 Helen, Finland

[#]Universidade de São Paulo, Rua do Matao, Travessa R, 185, 05508-900, Sao Paulo, SP, Brazil

[▽]Department of Technology, Metropolia University of Applied Sciences, P.O. Box 4000, FI-00180 Helsinki, Finland

[○]VTT Technical Research Centre of Finland, Fine Particles, P.O. Box 1000, FI-02044 VTT, Espoo, Finland

ⓈSupporting Information

ABSTRACT: Particle emissions affect radiative forcing in the atmosphere. Therefore, it is essential to know the physical and chemical characteristics of them. This work studied the chemical, physical, and optical characteristics of particle emissions from small-scale wood combustion, coal combustion of a heating and power plant, as well as heavy and light fuel oil combustion at a district heating station. Fine particle (PM_1) emissions were the highest in wood combustion with a high fraction of absorbing material. The emissions were lowest from coal combustion mostly because of efficient cleaning techniques used at the power plant. The chemical composition of aerosols from coal and oil combustion included mostly ions and trace elements with a rather low fraction of absorbing material. The single scattering albedo and aerosol forcing efficiency showed that primary particles emitted from wood combustion and some cases of oil combustion would have a clear climate warming effect even over dark earth surfaces. Instead, coal combustion particle emissions had a cooling effect. Secondary processes in the atmosphere will further change the radiative properties of these emissions but are not considered in this study.

INTRODUCTION

Combustion sources from large scale power and heat production to small-scale wood combustion emit a substantial amount of particles into the atmosphere. These emissions both deteriorate air quality locally and affect climate globally due to intercontinental transport of polluted air masses.[1] According to the Intergovernmental Panel on Climate Change (IPCC), total direct radiative forcing is estimated to be negative for aerosol (-0.5 ± 0.4 W m^{-2}).[2] However, black carbon (BC) emitted from fossil fuel and biomass burning absorbs solar radiation effectively influencing atmospheric and surface forcing.[3−7] The warming effect of fossil fuel BC aerosols is estimated to be in the range between +0.2 and 0.5 W m$^{-2,2,8}$ even though the possibility of overestimation of this effect has been shown by Cappa et al.[9]

Previous studies have characterized particle emissions of various burning technologies fueled with wood, oil, or coal: particle chemical properties and size distributions are investigated for residential combustion appliances fueled with wood logs or pellets.[10−13] Studies of oil and coal combustion with differential qualities of fuels and burning technologies also give an overview of the chemical properties and size distributions of emission particles.[13−16] Bond et al.[14] studied climate-relevant properties of particles emitted from oil combustion. Former studies show that the differences in fuels, combustion processes, and related technologies have

significant influence on the amount and characteristics of emissions. However, most of the previous studies did not study physical and chemical properties of particles together with radiative forcing effects. These comparisons would enable the connections to the climatic influences.

The simulation studies indicate that the contribution of anthropogenic BC emitted from Europe is significant in Arctic areas.[17] Thus, it is important to characterize emissions of energy production in the northern hemisphere. Here, we studied the characteristics of primary particles emitted from small scale wood combustion, a heavy fuel oil-fired district heating station, and a coal-fired heating and power plant, which are widely used methods for energy production, especially in Finland. All these combustion processes and technologies can be seen as important on a global scale. The knowledge on how different technologies affect the characteristics of emission particles is important, from the viewpoint of global modeling but also from the viewpoint of emission reduction policies.

We analyzed the chemical composition and the number size distribution of emitted aerosol and, partly based on those, report the optical properties of particles and aerosol forcing efficiency of them. The secondary processes affecting particles in the ambient air were not taken into account.

■ EXPERIMENTAL METHODS

Combustion Technologies. The experiments included three combustion technologies: small-scale wood combustion (SSWC), a heavy fuel oil-fired district heating station (HFO-HS), and a coal-fired power plant (C-PP). A summary of the campaigns is shown in Table 1.

The SSWC tests were performed in a laboratory. The studied technologies were a conventional masonry heater (SSWC-MH) fueled with dry (moisture 10−13 wt %) birch log batches and a pellet boiler (SSWC-PB) fueled with wood pellets. A detailed description of the experimental setup is given in Tissari et al.[10] and Lamberg et al.,[11] of which in the latter, the cases EFC (efficient combustion) and CBC3/23 (conventional batch combustion) indicated the pellet boiler and masonry heater of this study.

The C-PP experiments were performed at a height of 35 m on the smokestack of a large heating and power plant. The combustion took place in a boiler fueled either with pulverized bituminous coal or a mixture of coal and wood pellets (pellets 4.5 ± 1.4% of fuel volume). The sulfur content of dry coal was on average (±standard deviation) 0.39 ± 0.06 wt %. The flue gas was cleaned by an electrostatic precipitator and a desulfurization plant (DSP) including fabric filters before entering the smokestack. The nominal power of the power plant was 300 MW. The following combustion cases were studied: pure coal with DSP (C+DSP), a mixture of coal and pellets with DSP (C+P+DSP), and mixture of coal and pellets without DSP (C+P+bypassDSP).

The HFO-HS experiments were made for a heavy fuel oil-fired boiler operating at different powers and with different fuels: 78 MW produced by HFO, 78 MW produced by HFO with water emulsion, and 120 MW (full power) produced by a mixture of HFO (84 wt %) and light fuel oil (LFO, 16 wt %). In the following sections, we refer to these operating conditions with the abbreviations HFO+78MW, HFO+E+78MW, and HFO+LFO+120MW. The sulfur contents of HFO and the mixture of HFO and LFO were 0.89 and 0.75 wt %, respectively. There was not any flue gas after-treatment before the particle measurements.

Table 1. Description of the Combustion Campaigns

campaign	combustion appliance description	fuel	status of the cleaning device	dilution method	dilution ratio	measured parameters
SSWC	conventional masonry heater, pellet boiler	birch logs as batches, wood pellet	no cleaning system	after DT (pellet) or DT+ED	89−133 or 1087−2445	$\sigma_{SP},^a \sigma_{AP},^b$ NSD/VSD/MSD,^{c} chemical composition of particles
C-PP	Tampella/Babcock boiler with 12 Tampella/Babcock Hitachi HTNR low-NOx burners	Russian coal or Russian coal mixed with wood pellet	electrostatic precipitator + desulfurization plant (DSP)	after FPS installed into smokestack, 35 m height	18−45	$\sigma_{SP},^a \sigma_{AP},^b$ NSD/VSD/MSD,^{c} chemical composition of particles
HFO-HS	WiTermo HTK hot water boiler, nominal power 120 MW	heavy and light fuel oil	no cleaning system	after FPS installed into flue gas tunnel after boiler	55−62	$\sigma_{SP},^a \sigma_{AP},^b$ NSD/VSD/MSD,^{c} chemical composition of particles

^{a}Scattering coefficient (Mm^{-1}). ^{b}Absorption coefficient (Mm^{-1}). ^{c}Number/volume/mass size distribution

Instrumentation and Analytical Techniques. In the SSWC campaign, the particle sampling and dilution were carried out with a dilution tunnel (DT) for filter samples and a combination of a DT and an ejector diluter (ED, DI-1000, Dekati Ltd.) for determination of the optical properties of particles (Table 1). A Dekati Fine Particle Sampler (FPS-4000, Dekati Ltd.) was used to dilute flue gases in the HFO-HS and C-PP campaigns (Table 1). It has to be noted that high dilution ratios of the SSWC campaign, especially when ED was used, could lead to higher evaporation of, e.g., volatile and semivolatile aerosols in comparison with other combustion campaigns.[18] The temperature of the sample air was ca. 20−25 °C when entering the instruments.

The characteristics of emission particles were studied in each campaign with versatile instrumentation. The summary of the instrumentation of the campaigns is given in Supporting Information (SI) Table S1.

The optical characteristic of submicrometer particles (PM$_1$, aerodynamic particle diameter $D_a < 1$ μm) was determined measuring scattering and absorption coefficients (σ_{SP} and σ_{AP} (Mm^{-1}), respectively) with a Nephelometer (TSI model 3563, TSI Inc.)[19] and a Multi-Angle Absorption Photometer at $\lambda = 637$ nm[20] (MAAP, Model 5012, Thermo Fisher Scientific Inc.)[21] or a Particle Soot Absorption Photometer (PSAP, Radiance Research).[22] In the SSWC campaign, five upper stages (7−11) of a Berner low pressure impactor (BLPI)[23] were used to remove particles larger than 1 μm (flow rate 25 l min^{-1}).[24] The HFO-HS and S-PP campaigns used cyclones (sharp cut cyclone SCC 1.829, BGI Inc., USA) to remove particles >1 μm from the sample flow (flow rate 11 l min^{-1}). The MAAP results were converted to BC mass concentrations (M_{BC}) using a mass absorption efficiency (MAE) of 6.6 m^2 g^{-1}.[21] In the SSWC campaign, M_{BC} was estimated on the basis of the MAE of the MAAP to get comparable results with other campaigns. M_{BC} measured with the MAAP/PSAP is actually influenced by all particles absorbing light in used wavelengths. In addition to BC absorption, also absorption of, e.g., iron oxide is significant in the visible wavelength region.[25] Iron is a typical component of coal and oil fuel.[16] Thus, BC is here considered to be an absorbing material that does not definitely indicate pure BC only.

The number and volume size distributions were measured using a Fast Mobility Particle Sizer (FMPS, model 3091, TSI Inc.),[26] an Aerodynamic Particle Sizer (APS, model 3321, TSI Inc.),[27] and two Scanning Mobility Particle Sizers (SMPS).[28,29] SMPSs were equipped with DMA 3071 and CPC 3775 and with DMA 3085 and CPC 3025 (TSI Inc.), respectively. The mobility diameters (D_p) measured by the SMPS/FMPS were converted to aerodynamic diameters (D_a) when combined with the APS and compared with MOUDI mass size distribution. D_a's measured by the APS were converted to D_p's for Mie model simulations of optical properties of emission particles. Densities used in conversions were 2.96 and 1.77 g cm^{-3} for the SSWC-PB and SSWC-MH cases. These values were calculated on the basis of PM$_1$ mass concentrations and total volume determined from volume size distributions. For the HFO-HS and C-PP campaigns, a density of 2.5 g cm^{-3} was used because there were lacking data between gravimetric analysis and size distribution results. Estimation of this density was based on the typical chemical composition of particle emissions of coal and HFO combustion. HFO and coal combustion emissions consist typically of trace metal (density 1.7−11.4 g cm^{-3}) and mineral components (density ∼1.5−3.0 g cm^{-3}).[15,16] Measured

aerodynamic particle size ranges in the SSWC-PB, SSWC-MH, HFO-HS, and C-PP campaigns were 0.01−0.9, 0.008−0.696, 0.016−19.8, and 0.01−19.8 μm, respectively.

In all of the campaigns, emissions and the chemical composition of PM$_1$ ($D_a < 1$ μm) were determined from the Polytetrafluoroethylene (PTFE, Millipore, 3.0 μm, FSLW04700)-filter samples collected by filtration using a combination of five upper stages (7−11) of a BLPI[23] and a filter cassette (Gelman Science; flow rate 25 l min^{-1}).[24] In the HFO-HS and C-PP campaigns, emission particles were also collected by a rotating nano-Micro-Orifice Uniform Deposit Impactor (nano-MOUDI model 125B, MSP Corporation; flow rate 10 l min^{-1}).[30,31] PTFE and polycarbonate filters (GTTP04700, 0.2 μm) were used as sampling substrates. Sampling times were 1−4 h, 1 h, and 3−36 h for the HFO-HS, SSWC, and C-PP campaigns, respectively.

Gravimetric and chemical analysis was done for the PM$_1$ samples. From the MOUDI samples only chemical size analysis was discussed. Because of the limited campaign times, in some cases there was only one filter sampling for certain combustion conditions leading to the possibility of uncertainties of these results. Uncertainty estimation of filter sampling is presented in SI Table S3, but the repeatability of the combustion conditions was not possible to evaluate. Major ions were analyzed for all of the campaigns, whereas trace elements were determined only for the HFO-HS and C-PP. Monosaccharide anhydrides (MAs) and water-soluble organic carbon (WSOC) converted to water-soluble particulate organic matter by a factor of 1.8 (WSPOM)[32] were analyzed from the PM$_1$ samples of the SSWC. Total POM of the PM$_1$ particles was determined only in the HFO-HS campaign.

Major ions of PM$_1$ and MOUDI samples were analyzed by ion chromatography (ICS-2000, Dionex Corp.)[33] from the PTFE and polycarbonate filter pieces. Elemental components of the PM$_1$ samples from the HFO-HS and C-PP campaigns were analyzed by an inductively coupled plasma mass spectrometer (ICP-MS; DRC II, Perkin-Elmer SCIEX) and an inductively coupled plasma optical emission spectrometer (ICP-OES; Vista Pro Radial, Varian Inc.).[34] Yields for elements ranged between 54% and 104%, and the results were corrected based on the yields. Some MOUDI samples from the C-PP campaign were analyzed for elements by an X-ray Fluorescence Spectrometer (Epsilon 5, PANalytical B.V.).[35] Analyzed components are presented in SI Table S2.

The MAs and WSOC emissions of the SSWC were analyzed using a high-performance anion-exchange chromatograph coupled with electrospray ionization to a quadrupole-mass spectrometer (HPAEC-MS, Dionex Corp.)[36] and a total carbon analyzer equipped with a high-sensitive catalyst (TOC-V$_{CPH}$, Shimadzu),[37] respectively. The POM of the HFO-HS campaign was determined using a high-resolution time-of-flight aerosol mass spectrometer (HR-ToF-AMS, Aerodyne Research Inc.).[38]

Data Analysis. All the results were corrected for the dilution (Table 1), converted to the NTP conditions (0 °C and 101.3 kPa) and normalized from the oxygen content in the flue gas to the oxygen content of each fuel (13% for wood and pellets, 3% for HFO and LFO, and 6% for coal) to enable comparable conditions for various combustion processes.[39] Particle mass and number concentrations were presented in relation to the energy input to the burning processes (mg MJ^{-1} or # MJ^{-1}) based on the standard SFS5624.[39] The principles of the standard are presented in the SI.

829

dx.doi.org/10.1021/es4028698 | Environ. Sci. Technol. 2014, 48, 827−836

The nephelometer and PSAP data suffer from the instrumental limitations. Thus, σ_{SP} and σ_{AP} data were corrected based on the methods shown by Anderson and Ogren[19] and Virkkula,[40] respectively. σ_{SP} measured at $\lambda = 700$ nm and σ_{AP} measured by the PSAP were interpolated logarithmically to the MAAP wavelength (637 nm).[41]

The wavelength dependence of scattering presented by the scattering Ångström exponent (α_{SP}) is related to the particle size: α_{SP} increases with decreasing particle size.[42−44] Here, α_{SP} was calculated for the wavelength range 450−637 nm. The single scattering albedo (ω_0), that is, the ratio of σ_{SP} to the sum of σ_{SP} and σ_{AP} (extinction coefficient, σ_{EP}), was calculated based on the corrected σ_{SP} and σ_{AP} at a wavelength of 637 nm. It is an important factor in the estimations of radiative forcing of the aerosol particles.[45]

Furthermore, the mass extinction efficiency (MEE), which is dependent on particle size composition and size distribution, was calculated based on the ratio of σ_{EP} to PM_1.[46] Accurate estimates of MEE are important when computing the radiative forcing effects of aerosols and in the chemical extinction budgets used for the visibility regulatory purposes.[46]

The optical properties of the SSWC campaign were in addition simulated by Mie Model in SI section 2.2 to ensure the validity of the measured values.

Radiative forcing influence of emission particles was assessed by aerosol forcing efficiency ($\Delta F/\delta$, i.e., aerosol forcing per unit optical depth, W m^{-2}):[47−49]

$$\frac{\Delta F}{\delta} = -DS_0 T_{at}^2 (1 - A_c) \omega_0 \beta \left\{ (1 - R_s)^2 - \left(\frac{2R_s}{\beta} \right) \right.$$

$$\left. \left[\left(\frac{1}{\omega_0} \right) - 1 \right] \right\} \tag{1}$$

where D is the fractional day length, S_0 is the solar constant, T_{at} is the atmospheric transmission, A_c is the fractional cloud amount, R_s is the surface reflectance, and β is the average upscatter fraction calculated from hemispheric backscatter ratio b (backscattering-to-scattering) based on formula $\beta = 0.817 + 1.8495b - 2.9682b^2$.[48] Here, $\Delta F/\delta$ was estimated for each of the combustion cases using the average values of ω_0 and b for 637 nm. The constants used were $D = 0.5$, $S_0 = 1370$W m^{-2}, $T_{at} = 0.76$, $A_c = 0.6$, and $R_s = 0.15$, as suggested by Haywood and Shine.[50] The $\Delta F/\delta$ was further estimated in the relation to the average value of produced energy in an hour (W m^{-2}MJ^{-1}). This describes forcing efficiency in a cubic meter filled with aerosol mass emitted by 1 MJ of produced energy.

RESULTS AND DISCUSSION

Mass Concentration and Chemistry. Emissions of the analyzed and weighed PM_1 are summarized in Table 2 ($E_{A,PM1}$ and $E_{W,PM1}$ (mg MJ^{-1}), respectively). Detailed results of the analyzed components are presented in SI Table S4. Mass closures for the PM_1 of the studied combustion cases are shown in Figure 1. In this study, the used analytical techniques limited the possibility to reach the total PM_1 mass closure. In the SSWC-PB, analyzed mass covered 63 ± 7% of PM_1. In the SSWC-MH, analyzed mass was larger than weighed PM1 indicating uncertainty in analysis techniques or estimation of M_{BC}. In the HFO-HS and C-PP, the coverage of the total mass varied from 32 to 89%. The missing mass in these campaigns could include some nonanalyzed elements such as silicon (Si)

Table 2. Average (± Standard Deviation (stdev)) Emissions of the Analyzed PM_1 ($E_{A, PM1}$), Weighed PM_1 ($E_{W,PM1}$), and Number Emissions of the Fine and Coarse Particles Measured by the SMPS/FMPS and APS ((N_F, N_C, Respectively) for the Combustion Cases[a]

combustion case	$E_{A,PM1}$ (mg MJ^{-1})	$E_{W,PM1}$ (mg MJ^{-1})	N_F (# MJ^{-1})	N_C (# MJ^{-1})
SSWC-PB	11 ± 1	17.4 ± 2	$3.6 \times 10^{13} \pm 1.9 \times 10^{12}$	
SSWC-MH	40 ± 12	39 ± 2	$6.9 \times 10^{13} \pm 2.2 \times 10^{13}$	
C+DSP	0.16 ± 0.04	0.18 ± 0.06	$2.3 \times 10^9 \pm 4.0 \times 10^8$	$4.8 \times 10^8 \pm 1.9 \times 10^8$
C+P+DSP	0.10 ± 0.01	0.15 ± 0.02	$7.2 \times 10^{10} \pm 4.8 \times 10^{10}$	$1.6 \times 10^8 \pm 8.3 \times 10^7$
C+P+bypassDSP	0.4*	1.3*	$6.7 \times 10^{10} \pm 2.1 \times 10^{10}$	$1.2 \times 10^9 \pm 4.1 \times 10^8$
HFO+78MW	1.8*	3.1*	$1.1 \times 10^{13} \pm 1.2 \times 10^{11}$	$1.1 \times 10^8 \pm 3.3 \times 10^7$
HFO+E+78 MW	2.1*	3.6*	$1.1 \times 10^{13} \pm 1.2 \times 10^{11}$	$1.2 \times 10^8 \pm 1.5 \times 10^7$
HFO+LFO+ 120 MW	1.4*	2.3*	$1.0 \times 10^{13} \pm 1.7 \times 10^{11}$	$6.5 \times 10^7 \pm 1.8 \times 10^7$

[a]The aerodynamic size ranges of the N_F based on the FMPS/SMPS measurements were 0.01−0.9, 0.008−0.696, 0.016−0.26, and 0.016−0.655 nm for the SSWC-PB, SSWC-MH, C-PP, and HFO-HS experiments.

that occur especially in coal. Silicon is, e.g., in the form of quartz (SiO_2), aluminosilicate, or aluminosilicate salt.[51] In addition, oil and coal include a significant amount of trace metals that could form metallic oxides in the flue gas.[16,51,52] Oxygen in these compounds could explain part of the missing mass.

In general, the SSWC emitted the highest PM_1 emissions when compared with the C-PP and HFO-HS campaign (Table 2). This is reasonable because the combustion technique is not as advanced in small scale appliances as in larger scale boilers. The E_{PM1}'s were lowest in the C-PP, even in the case of the DSP bypassing. Also in this case, the flue gases passed the electrostatic precipitator, resulting in a significant decrease of particulate emissions when compared with the raw flue gas. Instead, the SSWC and HFO-HS did not have any cleaning system.

Most of the chemical components have scattering influence (e.g., sulfates and many organic compounds). The absorbing part is usually proposed to be BC but can also include, e.g., iron oxides that are highly absorbing in UV and visible light wavelengths and occur in oil and coal combustion flue gases.[15,16,25] Instead, in wood fuels, iron is not such a significant component.[11] In the SSWC-PB and SSWC-MH cases, contributions of absorbing material to PM_1 were 0.4 ± 0.2% and 94 ± 28%, respectively. The results of the absorbing material and iron were both summed to the analyzed mass as individual components. Thus, they might overlap if iron was in the form of iron oxides. In the HFO-HS campaign, the contribution of iron and absorbing material to the PM_1 was on average 3.3 ± 0.1% and 0.8 ± 0.2%, respectively. The iron contribution to the PM_1 was 0.2 ± 0.04% and 1.4% for the C+DSP and C+P+bypassDSP, respectively. The absorbing material contributed 3.7 ± 0.4% of the PM_1 in the C+DSP and 16% in the C+P+bypassDSP. The influence of absorption of iron oxides was tested assuming iron to be in the form of ferric oxide (Fe_2O_3) and MAE to be 0.56 m^2 g$^{-1(25)}$. The process and results are presented in the SI (section 2.1). The test results showed that for the HFO-HS campaign, absorption
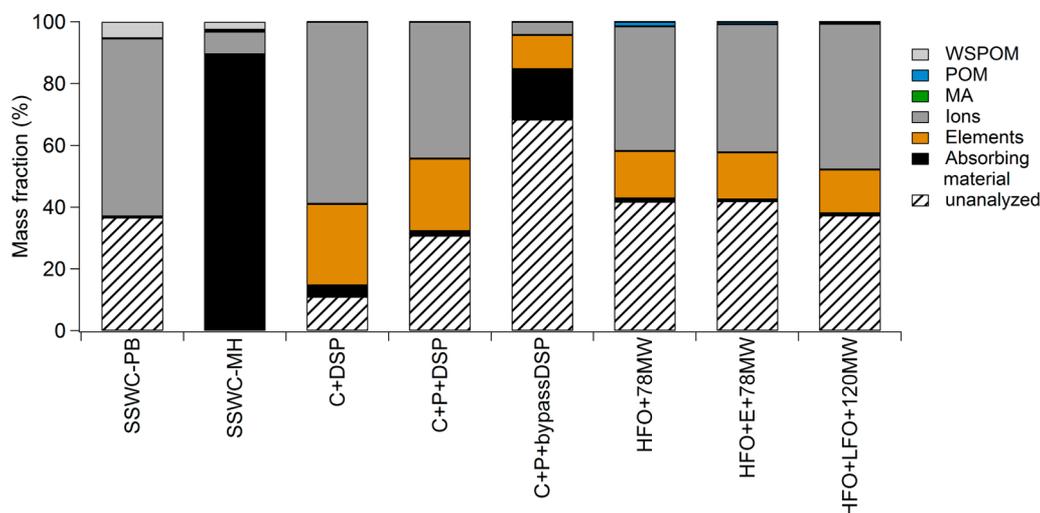
Figure 1. Mass closure of the PM_1 ($D_a < 1$ μm) in various combustion cases. Mass fractions of the bars from the SSWC-PB to the C+P+DSP are based on the average values of 2−5 filter samples. The results of the bars from the C+P+bypassDSP to the HFO+LFO+120MW represent mass fractions of only one filter sample in each case.

of Fe_2O_3 was in the range measured by the MAAP, whereas in the C-PP campaign this absorption contributed only some per cent of the measured absorption.

WSPOM (excluding MAs) and MAs were analyzed only for the SSWC campaign. The MAs are specific tracer compounds for inefficient biomass combustion, and the release of MAs has been suggested to be dependent on the combustion conditions.[32,53] The fraction of WSPOM from the PM_1 was 5.3 ± 0.8% and 2.6 ± 0.9% in the SSWC-PB and SSWC-MH, respectively. The low WSPOM fraction in the SSWC-MH was surprising but was determined also by Lamberg et al.[11] The reason stayed unclear but could be speculated upon: for example, insufficient air supply could influence the formation of organics. In addition, during aging, oxidation would increase the POM fraction and the water solubility of particles in comparison with fresh emissions here.[54] The contribution of MAs to the PM_1 was clearly higher in the SSWC-MH (0.6 ± 0.2%) than in the SSWC-PB (0.01 ± 0.002%). A lower MA fraction in the SSWC-PB than in the SSWC-MH was reasonable: The continuous fuel feeding and controlled provide of air in pellet boiler lead to more constant and efficient burning conditions when compared to conventional masonry heater with uncontrolled air supply and intermittent fuel loading.

The POM emissions determined by the HR-ToF-AMS in the HFO-HS campaign were low for all three of the experiments. Due to the efficient combustion process (e.g., effective fuel spraying, high temperature, optimal air-to-fuel ratio), it is reasonable that the particles in the flue gas are rather formed from metallic oxides and sulfates than organic compounds and soot.[13] The POM fraction was the highest in the case of HFO +78MW (1.5%). It seemed that the full power run with HFO +LFO fuel and emulsion decreased the organic fraction, which indicates that the boiler operation was optimized to full power. The influence of emulsion on the decline of the POM fraction could be explained by the occurrence of a "micro-explosion" of evaporating water.[55] A "micro-explosion" creates numerous new autoignition centers of combustion, leading to more efficient burning.[55]

In the PM_1 emissions, ions including alkali metals comprised the majority of the mass in most of the studied combustion

cases. Also, elements, such as trace metals, had a high contribution to the analyzed mass in the HFO-HS and C-PP campaigns. For the SSWC campaign, elements were not analyzed. In the SSWC-MH, C+DSP, and HFO+78, the ions contributed 7 ± 2%, 59 ± 9%, and 40% to the PM_1, respectively. In the SSWC, the increase in the ion fraction correlated with better combustion technology: the ion fraction was higher in the SSWC-PB than in the SSWC-MH. In the high combustion temperature of the SSWC-PB, inorganic ash species first evaporate and form particles by homogeneous nucleation and subsequent condensation in the cooling flue gas.[13] Major ions in the SSWC were K^+, SO_4^{2-}, Cl^-, and Na^+. In the HFO-HS emissions, the ions-to-PM_1 and elements-to-PM_1 fractions varied from 40 to 47% and from 14 to 15%, respectively. SO_4^{2-} contributed on average 88 ± 1% to ions in the HFO-HS cases. The most significant elements were Fe, Ni, V, K, and Mg. These metals are common species of oil fuels.[16,52,56] In the C+DSP case, ions dominated the chemical composition of the emissions consisting of 59 ± 9% of the PM_1. SO_4^{2-} was the most abundant ionic compound (55 ± 8% from the PM_1). Elements contributed 26 ± 2% to the PM_1. The main reasons for the high ion fraction are the chemicals used in the DSP process. The analyzed fraction of the flue gas cleaned only with the electrostatic precipitator (C+P+bypassDSP, the analyzed fraction contained only 32% of the PM_1) contained mostly metals such as Al, Fe, Mg, K, and Ni and absorbing material (35 and 52% of the analyzed mass). When the DSP was in use, metallic components and absorbing material were effectively removed from the flue gas. Calcium hydroxide ($Ca(OH)_2$) and sodium chloride (NaCl) are added to the flue gas passing the DSP to decrease the emissions of sulfur dioxide gas (SO_2). In this study, SO_2 gas emissions were on average 240 ± 60 mg Nm^{-3} and 620 ± 230 mg Nm^{-3} for the C+P +DSP and C+P+bypassDSP cases, respectively (SI Table S3). Thus, the chemical reactions in the DSP resulted in a decrease of SO_2 and metal emissions and enhanced mass concentrations of ions such as Ca^{2+}, Na^+, Cl^-, and SO_4^{2-} compared with the DSP bypass.

Number Emissions and Size Distributions. The number emissions of fine and coarse particles (cut off size $D_a = 1$ μm) measured by the SMPS/FMPS and APS (N_F and N_C,
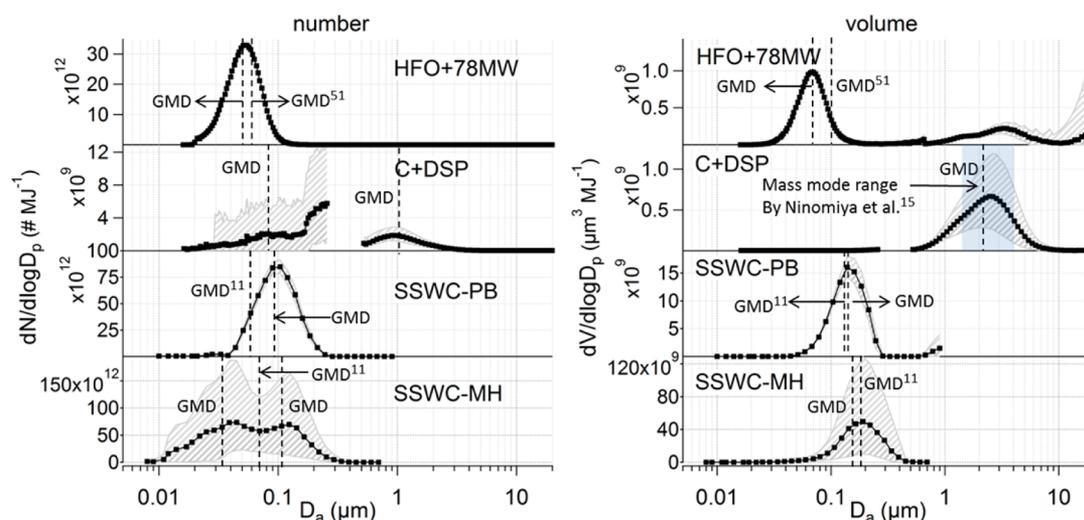
Figure 2. NSD (left) and VSD (right) of particle emissions of the SSWC-MH, SSWC-PB, HFO+78MW, and C+DSP cases. The *x*-axis particle diameter is aerodynamic. The distribution of the SSWC campaign includes only submicrometer range, whereas the size distributions of the HFO-HS and C-PP campaigns were determined by the APS up to 19.8 μm. The shaded areas represent 5 and 95 percentiles of size distributions, and dashed lines represent GMD$_a$'s measured in this study and presented by Lamberg et al.,[11] Ninomiya et al.,[15] and Tomeczek and Palugniok.[51]

respectively) are summarized in Table 2. As an example, Figure 2 presents number size distribution (NSD) and volume size distribution (VSD) of the cases SSWC-MH, SSWC-PB, HFO-78MW, and C+DSP. The size distributions of other cases are shown in SI Figure S2. Ion and element mass size distributions (MSD) of the C-PP campaign were determined from the MOUDI samples except for the C+P+bypassDSP where only ions were analyzed. For the HFO-HS campaign, ion MSDs were determined, but element MSD was not available.

Number emissions in the SSWC and HFO-HS were clearly higher than in the C-PP (Table 2). The most probable reason was the efficient cleaning system in the C-PP. Instead, the number emissions of the C-PP were emphasized in larger particles (Table 2, Figure 2).

The GMD$_a$'s of the wide bimodal NSD of the SSWC-MH were at 34 ± 7 and 113 ± 13 nm. The GMD$_a$ of the SSWC-MH volume size distribution was at 165 ± 29 nm. Instead, the NSD and VSD of the SSWC-PB were sharp and unimodal with GMDs at 94 ± 2 and 145 ± 9 nm, respectively. The width of the NSD and the number of the modes increased with the inefficiency of combustion. The VSD shifted to larger particles in the SSWC-MH when compared with the SSWC-PB case. The same behavior was observed in MSDs of these combustion appliances presented by Lamberg et al.[11]

The NSD of the HFO+78MW centered in the ultrafine particles with GMD$_a$ at 50 ± 0.2 nm. The distribution was sharp and in smaller particles when compared with the SSWC-MH and C+DSP cases. The amount of coarse particles was insignificant. In the VSD of the HFO+78MW, ultrafine and coarse modes were observed with GMD$_a$'s at 67 ± 3 nm and 3.5 ± 0.3 μm, respectively. An increase of volume concentration after 10 μm could indicate some unburned residual fly ash particles in the flue gas.[13] Also, the coarse mode between 1 and 10 μm was probably composed of residual particles. The ultrafine mode is expected to be formed via nucleation of vapor phase metal sulfates.[52] The size distributions agreed with the study of Sippula et al.,[13] which also presented the domination of the ultrafine mode in HFO combustion with a clear coarse mode in the MSD. Emulsion (HFO+E+78MW) shifted the ultrafine number mode slightly to larger particles and increased

N_C when compared with the HFO+78MW. Instead, the HFO +LFO+120MW case decreased N_C. Ion-MSD of the HFO +78MW peaked at the aerodynamic particle mean diameter 0.13 μm, being slightly larger in size than the ultrafine mode seen in VSD. Ions in particles <100 nm contributed 43%, 30% ,and 53% to PM$_{10}$ in the HFO+78MW, HFO+E+78MW, and HFO+LFO+120MW cases, respectively. The contribution of PM$_1$ to PM$_{10}$ varied only slightly in the range of 83−86%. Thus, combustion conditions seemed to affect more clearly ultrafine particles likely formed by vaporization−nucleation−condensation paths.

The role of coarse particles, especially in the VSD, was more significant in coal than in HFO combustion. In the C+DSP case, the NSD was bimodal with GMD$_a$'s at 81 ± 15 nm and 1.1 ± 0.1 μm. In addition, there seemed to be a mode forming in the end of the SMPS size distribution. The same behavior was observed in the C+P+bypassDSP but not in the C+P+DSP. The VSD of the C+DSP was dominated by coarse mode particles (GMD$_a$ 2.2 ± 0.2 μm) leading to a unimodal VSD. In the case of C+P+DSP, number and volume concentration of the ultrafine mode were clearly higher and the coarse mode lower than in the C+DSP case. The behavior could indicate better combustion of the mixed fuel, which is surprising because of the low content of the pellet. However, the inorganic ash species of the pellet probably evaporate easier than mineral components of coal and finally condensate to form ultrafine particles. The bypass of the DSP increased remarkably the number concentration of ultrafine particles, but the VSD was dominated by the coarse mode. Previous studies conducted in small-scale laboratory boilers without any cleaning techniques have also shown the domination of coarse particles in VSD or MSD.[15,16] Overall, coal combustion particles most probably form from inherent mineral matter within coal transferred into PM forming coarse particles and ultrafine and fine particles formed from vaporized and nucleated volatile metals.[15] The contribution of ultrafine particles to the VSDs of the C-PP campaign was overall unsubstantial. This was also seen in ion and element MSDs: the contribution of particles <100 nm to PM$_{10}$ was only 0.4−3%. Ion and element MSDs of the C+DSP peaked at 1.3 and 2.4

Table 3. Mass Extinction Efficiency (MEE), Scattering Ångström Exponent (α_{SP}), Single Scattering Albedo (ω_0), Radiative Forcing Efficiency ($\Delta F/\delta$), $\Delta F/\delta$ per Produced Energy ($\pm$ stdev), and Produced Energy of Studied Combustion Cases

combustion case	MEE (m^2 g^{-1})	α_{SP}	ω_0	$\Delta F/\delta$ (W m^{-2})	$\Delta F/\delta E$ (W m^{-2} MJ^{-1})	produced energy (MJ)
SSWC-PB	0.1 ± 0.02	3.8 ± 0.4	0.67 ± 0.13	−10 ± 10	−1 × 10^{-1} ± 1 × 10^{-1}	90
SSWC-MH	7.1 ± 7.9	2.2 ± 0.2	0.16 ± 0.08	34 ± 7	0.2 × 10^{-1} ± 4.9 × 10^{-2}	147
C+DSP	2.4 ± 0.9	1.3 ± 0.1	0.89 ± 0.05	−23 ± 4	−2 × 10^{-5} ± 4 × 10^{-6}	1080000
C+P+DSP	1.5 ± 0.5	1.8 ± 0.2	0.93 ± 0.06	−29 ± 5	−3 × 10^{-5} ± 5 × 10^{-6}	1080000
C+P+bypassDSP	3.3 ± 1.1	0.9 ± 0.03	0.65 ± 0.09	−6 ± 8	−5 × 10^{-6} ± 7 × 10^{-6}	1080000
HFO+78MW	0.2 ± 0.02	1.1 ± 0.1	0.57 ± 0.03	0.3 ± 3	1 × 10^{-6} ± 1 × 10^{-5}	256000
HFO+E+78MW	0.2 ± 0.01	2.1 ± 0.1	0.76 ± 0.02	−19 ± 1	−7 × 10^{-5} ± 6 × 10^{-6}	257000
HFO+LFO+ 120MW	0.1 ± 0.01	1.4 ± 0.1	0.52 ± 0.05	4 ± 4	1 × 10^{-5} ± 1 × 10^{-5}	370000
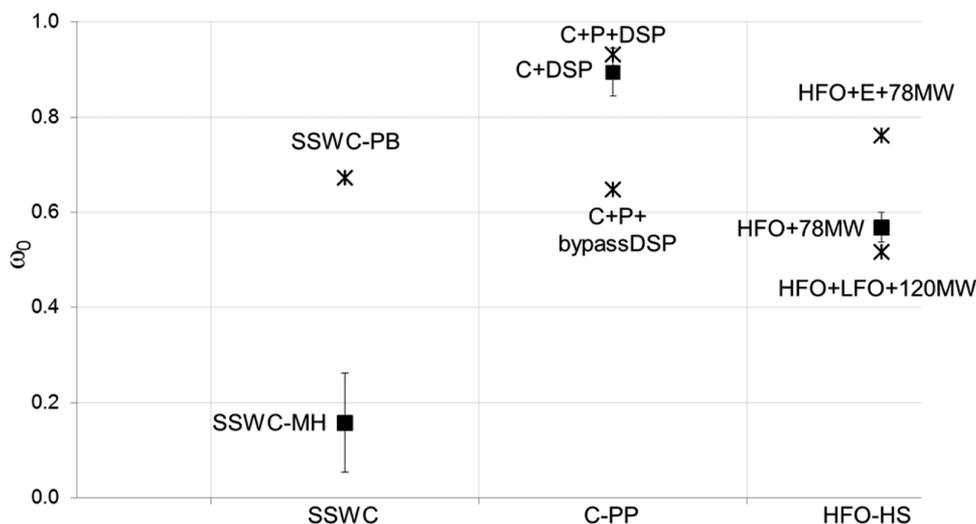
Figure 3. Single scattering albedo (ω_0) of the PM$_1$ emissions of various combustion technologies.

μm, respectively. In the C+P+DSP, the mode maximum was at 1.3 μm for both ion and element MSDs. For the DSP bypass, ion distribution peaked at 1.3 and 4.3 μm.

Optical Properties. The mean values ± stdev of the MEE, α_{SP}, and ω_0 are shown in Table 3. The influence of the optical properties of particles on radiative forcing was assessed based on the formula of $\Delta F/\delta$ (W m^{-2}; eq 1) and the average value of produced energy E in an hour. Also, these results are summarized in Table 3. In addition, optical properties of the SSWC campaign were also simulated by the Mie theory to see if the results were consistent. These supporting results were compiled in the SI. The MEE values were calculated in order to connect the optical properties with the PM$_1$ emissions. The MEE values of the SSWC-PB and HFO-HS campaign were rather low (ca. 0.1−0.2 m^2 g^{-1}). For the SSWC-PB, this result agreed with simulation results (SI Table S8). Also, Hand and Malm[46] reviewed the size distribution dependence of mass scattering efficiencies (MSE) that showed MSE values as low as 0.5 m^2 g^{-1} for the particles with an aerodynamic diameter of 0.2 μm. They showed that the trend of MSE was decreasing with decreasing particle sizes. Thus, for particles <0.2 μm, MSE could be even lower. The MEE of the SSWC-MH in the present study was 7.1 ± 7.9 m^2 g^{-1}. This value agreed with mass absorption efficiencies (MAE) published previously, e.g., by Petzold and Schönlinner[21] and Bond and Bergstrom.[57] The result is consistent with the fact that absorbing material composed 94 ± 28% of the PM$_1$ emissions of the SSWC-MH (Figure 1). The MEE values of the C-PP campaign were in the range of 1.5−3.3, which corresponds with the published MSE values for inorganic species (2.9 ± 0.3 m^2 g^{-1}).[58] As the

chemistry and the NSD and VSD results showed, argumentation of the MEE values was reasonable for the C-PP campaign.

Scattering Ångström exponent α_{SP} was discussed to relate scattering with the particle diameter. Overall, α_{SP} was the highest for the SSWC campaign (3.8 ± 0.4 and 2.2 ± 0.2 for the SSWC-PB and SSWC-MH, respectively). The NSD of the SSWC-PB was unimodal, whereas SSWC-MH distribution was multimodal, increasing the importance of particles larger than the mode maximum. Thus, a lower α_{SP} value for the SSWC-MH than for the SSWC-PB was reasonable. The lowest value of α_{SP} (0.9 ± 0.03) was found for the C+P+bypassDSP of the C-PP campaign. This is in accordance with the fact that particle NSD was in larger particles than in the other cases of the C-PP campaign. Even though there was a mode maximum in the ultrafine size range for the C-PP cases with DSP, Figure 2 showed that the number concentration was significant up to 1 μm. This fact stands for low α_{SP} values. α_{SP} values in the HFO-HS campaign were in the range of ca. 1.1−2.1. Even though the number concentration and particle mode maximum were nearly constant in the four combustion cases, the α_{SP} varied clearly. In general, the α_{SP} seemed to be dependent also on combustion technology and fuel. For example, the lowest values of the C-PP campaign were in agreement with the values presented for dust aerosol.[42] Both coal combustion particles and dust particles include a significant amount of mineral matter especially in the coarse mode. For submicrometer particles, the values of the scattering Ångström exponent around 1.5−1.8 for polluted urban aerosol have been reported.[43,44,59] Results of the HFO-HS experiments fit best with these values.

The average ($\pm$stdev) single scattering albedo ω_0 of the MS-SSWC, HFO+78MW, and C+DSP cases are shown in Figure 3 (black squares) and Table 3. ω_0's of the additional combustion cases are shown as black stars for more accurate speculation of the influence of the combustion conditions on ω_0. In the ambient air, ω_0 differs depending on the source and age of particles. In the study of Lyamani et al.,[59] ω_0 varied between 0.5 and 0.8 in an urban traffic influenced site. Instead, Carrico et al.[60] showed higher ω_0 values ($\sim$0.9) for urban aerosol. In nonpolluted regions, ω_0 is usually higher than 0.9, which represents particles consisting almost only of scattering material. The ω_0 of pure soot is approximately 0.3.[61] As Figure 3 shows, obvious differences in ω_0 were seen between the combustion campaigns and the cases inside them. The ω_0 of the HFO-HS campaign varied between 0.52 ± 0.05 and 0.76 ± 0.02. These values indicated a rather high absorbing influence of particles even though the fraction of absorbing material was rather low. The use of emulsion seemed to increase ω_0, which is in accordance with the fact that the emulsion should improve the combustion of the fuel. The ω_0 for the SSWC-PB (0.67 ± 0.13) was in the same range as for the HFO-HS campaign, and also in this case, the absorbing material-to-PM_1 ratio was low. This discrepancy could be explained by optical properties of size distributions of these cases: Figure S4 in the SI showed that for the SSWC-PB, absorption efficiencies of particles approximately <60 nm (mobility diameter) were higher than scattering efficiencies. A remarkable part of the particles was below this range. The shape and position of the size distributions of the HFO-HS campaign corresponded to the ones in the SSWC-PB case. Thus, the same behavior could be expected. The low ω_0 of the SSWC-MH (0.16 ± 0.10) was consistent with high BC fraction shown in Figure 1. As was shown by the study of Lamberg et al.,[11] in which the combustion technologies used corresponded to the ones in this study, the contribution of EC to PM_1 was highest for the masonry heater, which is in agreement with the ω_0 determined in this study. The C-PP campaign seemed to emit mostly scattering particles when DSP was used. The high fraction of ions with a high sulfate fraction endorsed high ω_0 values (Figure 1). The contribution of absorbing material increased with the bypass of the DSP corresponding to a significant decrease of ω_0 to 0.65 ± 0.09 (Figure 1, Table 3).

In the $\Delta F/\delta$ results, the negative and positive sign indicate a cooling and warming effect of the aerosol in question. The used surface reflectance, $R_s = 0.15$, represents a dark surface such as grass. Setting R_s to a value describing snow-covered ground (>0.6) would lead to higher values of $\Delta F/\delta$. $\Delta F/\delta$ values were negative (i.e., cooling effect) for all of the other cases but SSWC-MH, HFO+78MW, and HFO+LFO+120MW. As fresh aerosols, these cases would lead to the warming of the climate, with the SSWC-MH having clearly the strongest warming effect. The values of the C+DSP, C+P+DSP, and HFO+E+78MW were in the same range with the values presented by Virkkula et al.[49] This study reported values between -20 and -27 W m^{-2} for ambient background aerosol. Overall, if primary particle emissions of this study would transport to the areas with high ground reflectance (e.g., snow-covered Arctic), they would have a warming effect.

This study gives insight into characteristics of primary particle emissions of the described combustion techniques and possible radiative influence of these emissions that were not widely presented previously. The PM_1 emissions of wood combustion were highest and most influenced by absorbing

particles. Instead, the particle emissions from the C-PP seemed to have mainly a scattering influence and were clearly lower than in the SSWC and HFO-HS campaigns because of efficient burning and cleaning techniques. Emissions of coal and oil combustion were composed mostly of ions and trace elements including a low content of absorbing material. Interestingly, absorption of the HFO-HS emissions was rather high, and it was estimated to be influenced by iron oxide rather than black carbon. The same characteristic was seen in pellet boiler emissions. This could be explained by the high absorption efficiency of ultrafine particles of HFO-HS and SSWC-PB emissions. Overall, single scattering albedo and aerosol forcing efficiency showed that masonry heater and some HFO-HS emissions would have a warming effect on the climate with the assumptions done in this study. Overall, if primary particle emissions of this study would transport to the areas with high ground reflectance (e.g., snow-covered Arctic) as such they would have warming effect. However, these results represent primary emissions that will undergo further physical and chemical transformation in the atmosphere with aging.

■ ASSOCIATED CONTENT

Ⓢ Supporting Information
Determined quantities and instrument information of the combustion campaigns are presented in Table S1 and analyzed results of the chemical components of the combustion campaigns in Table S2. Additional tables (Tables S3−S11) and figures (Figures S1−S5) are also included. This information is available free of charge via the Internet at http://pubs.acs.org.

■ AUTHOR INFORMATION

Corresponding Author
*Phone: +358 05 566 5104. Fax: +358 29 539 5403. E-mail: anna.frey@fmi.fi.

Notes
The authors declare no competing financial interest.

■ REFERENCES

(1) Flanner, M. G.; Zender, C. S.; Randerson, J. T.; Rasch, P. J. Present-day climate forcing and response from black carbon in snow. *J. Geophys. Res.* **2007**, *112* (D11202), DOI: 10.1029/2006JD008003.
(2) *IPCC, 2007: Climate Change 2007: The Physical Science Basis*, Contribution of Working Group I to the Fourth Assessment Report of the Intergovernmental Panel on Climate Change; Solomon, S., Qin, D., Manning, M., Chen, Z., Marquis, M., Averyt, K. B., Tignor, M., Miller, H. L., Eds.; Cambridge University Press: Cambridge, United Kingdom, 2007.
(3) Podgorny, I. A.; Conant, W. C.; Ramanathan, V.; Satheesh, S. K. Aerosol modulation of atmospheric and surface solar heating rates over the tropical Indian Ocean. *Tellus B* **2000**, *52*, 947−958 , DOI: DOI: 10.1034/j.1600-0889.2000.d01-4.x.
(4) Shindell, D.; Kuylenstierna, J.; Vignati, E.; van Dingenen, R.; Amann, M.; Klimont, Z.; Anenberg, S.; Muller, N.; Janssens-Maenhout, G.; Raes, F.; Schwartz, J.; Faluvegi, G.; Pozzoli, L.; Kupiainen, K.; Höglund-Isaksson, L.; Emberson, L.; Streets, D.;

Ramanathan, V.; Hicks, K.; Oanh, N. T. K.; Milly, G.; Williams, M.; Demkine, V.; Fowler, D. Simultaneously mitigating near-term climate change and improving human health and food security. *Science* **2012**, *335*, 183−189 , DOI: DOI: 10.1126/science.1210026.

(5) Hansen, J.; Nazarenko, L. Soot climate forcing via snow and ice albedos. *Proc. Natl. Acad. Sci. U. S. A.* **2004**, *101*, 423−428.

(6) Koch, D.; Hansen, J. Distant origins of Arctic black carbon: A Goddard Institute for Space Studies ModelE experiment. *J. Geophys. Res.* **2005**, *110* (D04204), DOI: 10.1029/2004JD005296.

(7) Ramanathan, V.; Carmichael, G. Global and regional climate changes due to black carbon. *Nature* **2008**, *1*, 221−227 , DOI: DOI: 10.1038/ngeo156.

(8) Jacobson, M. Z. Strong radiative heating due to the mixing state of black carbon in atmospheric aerosols. *Nature* **2001**, *409*, 695−697 , DOI: DOI: 10.1038/35055518.

(9) Cappa, C.; Onasch, T.; Massoli, P.; Worsnop, D.; Bates, T.; Cross, E.; Davidovits, P.; Hakala, J.; Hayden, K.; Jobson, B.; Kolesar, K.; Lack, D.; Lerner, B.; Li, S.-M.; Mellon, D.; Nuaaman, I.; Olfert, J.; Petäjä, T.; Quinn, P.; Song, C.; Subramanian, R.; Williams, E.; Zaveri, R. Radiative absorption enhancements due to the mixing state of atmospheric black carbon. *Science* **2012**, *337*, 1078−1081 , DOI: DOI: 10.1126/science.1223447.

(10) Tissari, J.; Hytönen, K.; Sippula, O.; Jokiniemi, J. The effects of operating conditions on emissions from masonry heaters and sauna stoves. *Biomass Bioenergy* **2009**, *33*, 513−520 , DOI: DOI: 10.1016/j.biombioe.2008.08.009.

(11) Lamberg, H.; Nuutinen, K.; Tissari, J.; Ruusunen, J.; Yli-Pirilä, P.; Sippula, O.; Tapanainen, M.; Jalava, P.; Makkonen, U.; Teinilä, K.; Saarnio, K.; Hillamo, R.; Hirvonen, M.-R.; Jokiniemi, J. Physicochemical characterization of fine particles from small-scale wood combustion. *Atmos. Environ.* **2011**, *45*, 7635−7643 , DOI: DOI: 10.1016/j.atmosenv.2011.02.072.

(12) Johansson, L. S.; Leckner, B.; Gustavsson, L.; Cooper, D.; Tullin, C.; Potter, A. Emission characteristics of modern and old-type residential boilers fired with wood logs and wood pellets. *Atmos. Environ.* **2004**, *38* (25), 4183−4195 , DOI: DOI: 10.1016/j.atmosenv.2004.04.020.

(13) Sippula, O.; Hokkinen, J.; Puustinen, H.; Yli-Pirila, P.; Jokiniemi, J. Comparison of particle emissions from small heavy fuel oil and wood-fired boilers. *Atmos. Environ.* **2009**, *43*, 4855−4864 , DOI: DOI: 10.1016/j.atmosenv.2009.07.022.

(14) Bond, T. C.; Wehner, B.; Plewka, A.; Wiedensohler, A.; Heintzenberg, J.; Charlson, R. J. Climate-relevant properties of primary particulate emissions from oil and natural gas combustion. *Atmos. Environ.* **2006**, *40* (19), 3574−3587 , DOI: DOI: 10.1016/j.atmosenv.2005.12.030.

(15) Ninomiya, Y.; Zhang, L.; Sato, A.; Dong, Z. Influence of coal particle size on particulate matter emission and its chemical species produced during coal combustion. *Fuel Process. Technol.* **2004**, *85*, 1065−1088 , DOI: DOI: 10.1016/j.fuproc.2003.10.012.

(16) Linak, W.; Miller, C. A.; Wendt, J. Comparison of particle size distributions and elemental partitioning from the combustion of pulverized coal and residual fuel oil. *J. Air Waste Manage. Assoc.* **2000**, *50* (8), 1532−1544 , DOI: DOI: 10.1080/10473289.2000.10464171.

(17) Huang, L.; Gong, S. L.; Jia, C. Q.; Lavoué, D. Relative contributions of anthropogenic emissions to black carbon aerosol in the Arctic. *J. Geophys. Res.* **2010**, *115* (D19208), DOI: 10.1029/2009JD013592.

(18) Robinson, A.; Donahue, N.; Shrivastava, M.; Weitkamp, E.; Sage, A.; Grieshop, A.; Lane, T.; Pierce, J.; Pandis, S. Rethinking organic aerosols: Semivolatile emissions and photochemical aging. *Science* **2007**, *315*, 1259−1262 , DOI: DOI: 10.1126/science.1133061.

(19) Anderson, T.; Ogren, J. Determining aerosol radiative properties using the TSI 3563 integrating nephelometer. *Aerosol Sci. Technol.* **1998**, *29*, 57−69 , DOI: DOI: 10.1080/02786829808965551.

(20) Müller, T.; Henzing, J. S.; de Leeuw, G.; Wiedensohler, A.; Alastuey, A.; Angelov, H.; Bizjak, M.; Collaud Coen, M.; Engström, J. E.; Gruening, C.; Hillamo, R.; Hoffer, A.; Imre, K.; Ivanow, P.;

Jennings, G.; Sun, J. Y.; Kalivitis, N.; Karlsson, H.; Komppula, M.; Laj, P.; Li, S.-M.; Lunder, C.; Marinoni, A.; Martins dos Santos, S.; Moerman, M.; Nowak, A.; Ogren, J. A.; Petzold, A.; Pichon, J. M.; Rodriquez, S.; Sharma, S.; Sheridan, P. J.; Teinilä, K.; Tuch, T.; Viana, M.; Virkkula, A.; Weingartner, E.; Wilhelm, R.; Wang, Y. Q. Characterization and intercomparison of aerosol absorption photometers: result of two intercomparison workshops. *Atmos. Meas. Tech.* **2011**, *4*, 245−268 , DOI: DOI: 10.5194/amt-4-245-2011.

(21) Petzold, A.; Schönlinner, M. Multi-angle absorption photometry − a new method for the measurement of aerosol light absorption and atmospheric black carbon. *Aerosol Sci.* **2004**, *35*, 421−441 , DOI: DOI: 10.1016/j.jaerosci.2003.09.005.

(22) Bond, T.; Anderson, T.; Campbell, D. Calibration and intercomparison of filter-based measurements of visible light absorption by aerosols. *Aerosol Sci. Technol.* **1999**, *30*, 582−600 , DOI: DOI: 10.1080/027868299304435.

(23) Berner, A.; Lürzer, C. Mass size distributions of traffic aerosols at Vienna. *J. Phys. Chem.* **1980**, *84*, 2079−2083 , DOI: DOI: 10.1021/j100453a016.

(24) Saarikoski, S.; Timonen, H.; Saarnio, K.; Aurela, M.; Järvi, L.; Keronen, P.; Kerminen, V.-M.; Hillamo, R. Sources of organic carbon in fine particulate matter in northern European urban air. *Atmos. Chem. Phys.* **2008**, *8*, 6281−6295 , DOI: DOI: 10.5194/acp-8-6281-2008.

(25) Alfaro, S.;Lafon, S., Rajot, J.; Formenti, P.; Gaudichet, A.; Maillé, M. Iron oxides and light absorption by pure desert dust: An experimental study. *J. Geophys. Res.* **2004**, *109* (D08208), DOI:10.1029/2003JD004374.

(26) Tammet, H.; Mirme, A.; Tamm, E. Electrical Aerosol Spectrometer of Tartu University. *Atmos. Res.* **2002**, *62*, 315−324, DOI: 10.1016/S0169-8095(02)00017-0.

(27) Peters, T. M.; Leith, D. Concentration measurement and counting efficiency of the aerodynamic particle sizer 3321. *Aerosol Sci.* **2003**, *34*, 627−634 , DOI: DOI: 10.1016/S0021-8502(03)00030-2.

(28) Wang, S. C.; Flagan, R. C. Scanning Electrical Mobility Spectrometer. *Aerosol Sci. Technol.* **1990**, *13*, 230−240 , DOI: DOI: 10.1080/02786829008959441.

(29) Chen, D.-R.; Pui, D.; Hummes, D.; Fissan, H.; Quant, F.; Sem, G. Design and Evaluation of a Nanometer Aerosol Differential Mobility Analyzer (Nano-DMA). *J. Aerosol Sci.* **1998**, *29*, 497−509 , DOI: DOI: 10.1016/S0021-8502(97)10018-0.

(30) Marple, V. A.; Rubow, K. L.; Behm, S. M. A Microorifice Uniform Deposit Impactor (MOUDI): Description, Calibration, and Use. *Aerosol Sci. Technol.* **1991**, *14* (4), 434−446 , DOI: DOI: 10.1080/02786829108959504.

(31) Marple, V. A.; Olson, B. A. *A Micro-Orifice Impactor with Cut Sizes Down to 10 Nanometers for Diesel Exhaust Sampling*; Final Report Generic Center for Respirable Dust, Pennsylvania State University: University Park, PA, 1999.

(32) Frey, A.; Tissari, J.; Saarnio, K.; Timonen, H.; Tolonen-Kivimäki, O.; Aurela, M.; Saarikoski, S.; Makkonen, U.; Hytönen, K.; Jokiniemi, J.; Salonen, R. O.; Hillamo, R. Chemical Composition and Mass Size Distribution of Fine Particulate Matter Emitted by a Small Masonry Heater. *Boreal Env. Res.* **2009**, *14*, 225−271.

(33) Timonen, H.; Aurela, M.; Carbone, S.; Saarnio, K.; Saarikoski, S.; Mäkelä, T.; Kulmala, M.; Kerminen, V.-M.; Worsnop, D. R.; Hillamo, R. High time-resolution chemical characterization of the water-soluble fraction of ambient aerosols with PILS-TOC-IC and AMS. *Atm. Meas. Tech.* **2010**, *3*, 1063−1074 , DOI: DOI: 10.5194/amt-3-1063-2010.

(34) Danadurai, K. S. K.; Chellam, S.; Lee, C.-T; Fraser, M. P. Trace elemental analysis of airborne particulate matter using dynamic reaction cell inductively coupled plasma - mass spectrometry: Application to monitoring episodic industrial emission events. *Anal. Chim. Acta* **2011**, *686*, 40−49 , DOI: DOI: 10.1016/j.aca.2010.11.037.

(35) Van Meel, K.; Smekens, A.; Behets, M.; Kazandjian, P.; Van Grieken, R. Determination of Platinum, Palladium, and Rhodium in Automotive Catalysts Using High-Energy Secondary Target X-ray

Fluorescence Spectrometry. *Anal. Chem.* **2007**, *79*, 6383−6389 , DOI: DOI: 10.1021/ac070815r.

(36) Saarnio, K.; Teinilä, K.; Aurela, M.; Timonen, H.; Hillamo, R. High-performance anion-exchange chromatography−mass spectrometry method for determination of levoglucosan; mannosan, and galactosan in atmospheric fine particulate matter. *Anal. Bioanal. Chem.* **2010**, *398*, 2253−2264 , DOI: DOI: 10.1007/s00216-010-4151-4.

(37) Timonen, H.; Saarikoski, S.; Aurela, M.; Saarnio, K.; Hillamo, R. Water-soluble organic carbon in urban aerosol: concentrations, size distributions and contribution to particulate matter. *Boreal Env. Res.* **2008**, *13*, 335−346.

(38) DeCarlo, P. F.; Kimmel, J. R.; Trimborn, A.; Northway, M. J.; Jayne, J. T.; Aiken, A. C.; Gonin, M.; Fuhrer, K.; Horvath, T.; Docherty, K. S.; Worsnop, D. R.; Jimenez, J. L. Field-deployable, high-resolution, time-of-flight mass spectrometer. *Anal. Chem.* **2006**, *78*, 8281−8289 , DOI: DOI: 10.1080/027868290903907.

(39) *SFS 5624: Air Quality. Stationary Source Emissions. Determination of the Flue Gas Conditions, 1990*; Finnish Standards Association SFS, Helsinki, Finland, 1990.

(40) Virkkula, A. Correction of the calibration of the 3-wavelength Particle Soot Absorption Photometer (3λ PSAP). *Aerosol Sci. Technol.* **2010**, *44*, 706−712 , DOI: DOI: 10.1080/02786826.2010.482110.

(41) Virkkula, A.; Ahlquist, N.; Covert, D.; Sheridan, P.; Arnott, W.; Ogren, J. A three-wavelength optical extinction cell for measuring aerosol light extinction and its application to determining light absorption coefficient. *Aerosol Sci. Technol.* **2005**, *39*, 52−67 , DOI: DOI: 10.1080/027868290901918.

(42) Eck, T.; Holben, B.; Reid, J.; Dubovik, O.; Smimov, A.; O'Neill, N.; Slutsker, I.; Kinne, S. Wavelength dependence of the optical depth of biomass burning; urban; and desert dust aerosols. *J. Geophys. Res.* **1999**, *104* (D24), 31333−31349 , DOI: DOI: 10.1029/1999JD900923.

(43) Doherty, S.; Quinn, P.; Jefferson, A.; Carrico, C.; Anderson, T.; Hegg, D. A comparison and summary of aerosol optical properties as observed in situ from aircraft, ship, and land during ACE-Asia. *J. Geophys. Res.* **2005**, *110* (D04201), DOI: 10.1029/2004JD004964.

(44) Pereira, S.; Wagner, F.; Silva, A. Seven years of measurements of aerosol scattering properties, near the surface, in the southwestern Iberia Peninsula. *Atmos. Chem. Phys.* **2011**, *11*, 17−29 , DOI: DOI: 10.5194/acp-11-17-2011.

(45) Takemura, T.; Nakajima, T.; Dubovik, O.; Holben, B.; Kinne, S. Single-scattering albedo and radiative forcing of various aerosol species with a global three-dimensional model. *J. Clim.* **2002**, *15*, 333−352 , DOI: DOI: 10.1175/1520-0442(2002)015<0333:SSAARF>2.0.-CO;2.

(46) Hand, J. L.; Malm, W. C. Review of aerosol mass scattering efficiencies from ground-based measurements since 1990. *J. Geophys. Res.* **2007**, *112* (D16203), DOI: 10.1029/2007JD008484.

(47) Sheridan, P. J.; Ogren, J. A. Observations of the vertical and regional variability of aerosol optical properties over central and eastern North America. *J. Geophys. Res.* **1999**, *104*, 16793−16805 , DOI: DOI: 10.1029/1999JD900241.

(48) Delene, D. J.; Ogren, J. A. Variability of aerosol optical properties at four North American surface monitoring sites. *J. Atmos. Sci.* **2002**, *59*, 1135−1150.

(49) Virkkula, A.; Backman, J.; Aalto, P. P.; Hulkkonen, M.; Riuttanen, L.; Nieminen, T.; dal Maso, M.; Sogacheva, L.; de Leeuw, G.; Kulmala, M. Seasonal cycle, size dependencies, and source analyses of aerosol optical properties at the SMEAR II measurement station in Hyytiälä, Finland. *Atmos. Chem. Phys.* **2011**, *11*, 4445−4468 , DOI: DOI: 10.5194/acp-11-4445-2011.

(50) Haywood, J. M.; Shine, K. P. The effect of anthropogenic sulfate and soot aerosol on the clear sky planetary radiation budget. *Geophys. Res. Lett.* **1995**, *22* (4), 603−606 , DOI: DOI: 10.1029/95GL00075.

(51) Tomeczek, J.; Palugniok, H. Kinetics of mineral matter transformation during coal combustion. *Fuel* **2002**, *81*, 1251−1258 , DOI: DOI: 10.1016/S0016-2361(02)00027-3.

(52) Linak, W.; Miller, C.; Wendt, J. Fine particle emissions from residual fuel oil combustion: characterization and mechanism of formation. *Proc. Combust. Inst.* **2000**, *28*, 2651−2658 , DOI: DOI: 10.1016/S0082-0784(00)80684-0.

(53) Saarnio, K.; Niemi, J.; Saarikoski, S.; Aurela, M.; Timonen, H.; Teinilä, K.; Myllynen, M.; Frey, A.; Lamberg, H.; Jokiniemi, J.; Hillamo, R. Using monosaccharide anhydrides to estimate the impact of wood combustion in fine particles in Helsinki Metropolitan Area. *Boreal Env. Res.* **2012**, *17*, 163−183.

(54) Jimenez, J.; Canagaratna, M.; Donahue, N. Evolution of organic aerosols in the atmosphere. *Science* **2009**, *326*, 1525−1529 , DOI: DOI: 10.1126/science.1180353.

(55) Fu, W.; Hou, L.; Wang, L.; Ma, F. A unified model for the micro-explosion of emulsified droplets of oil and water. *Fuel Process. Technol.* **2002**, *79*, 107−119 , DOI: DOI: 10.1016/S0378-3820(02)00106-6.

(56) Wang, Y.; Chao, H.; Wang, L.; Chang-Chien, G.; Tsou, T.. Characteristics of heavy metals emitted from a heavy oil-fueled power plant in northern Taiwan. *Aerosol Air Qual. Res.* **2010**, *10*, 111−118 , DOI: DOI: 10.4209/aaqr.2009.09.0056.

(57) Bond, T. C.; Bergstrom, R. W. Light Absorption by Carbonaceous Particles: An Investigative Review. *Aerosol Sci. Technol.* **2006**, *40* (1), 27−67 , DOI: DOI: 10.1080/02786820500421521.

(58) Malm, W. C.; Hand, J. L. An examination of the physical and optical properties of aerosols collected in the IMPROVE program. *Atmos. Environ.* **2007**, *41*, 3407−3427 , DOI: DOI: 10.1016/j.atmosenv.2006.12.012.

(59) Lyamani, H.; Olmo, F.; Alados-Arboledas, L. Light scattering and absorption properties of aerosol particles in the urban environment of Granada, Spain. *Atmos. Environ.* **2008**, *42*, 2630−2642 , DOI: DOI: 10.1016/j.atmosenv.2007.10.070.

(60) Carrico, C.; Bergin, M.; Xu, J.; Baumann, K.; Maring, H. Urban aerosol radiative properties: Measurements during the 1999 Atlanta Supersite Experiment. *J. Geophys. Res.* **2003**, *108* (D7), 8422 , DOI: DOI: 10.1029/2001JD001222.

(61) Mikhailov, E.; Vlasenko, S.; Podgorny, I.; Ramanathan, V.; Corrigan, C. Optical properties of soot-water drop agglomerates: An experimental study. *J. Geophys. Res.* **2006**, *111*, 1−16 , DOI: DOI: 10.1029/2005JD006389.

836

dx.doi.org/10.1021/es4028698 | *Environ. Sci. Technol.* 2014, 48, 827−836